Annu. Rev. Fluid Mech. 2000. 32:241–274

CAPILLARY EFFECTS ON SURFACE WAVES

Marc Perlin and William W. Schultz
Naval Architecture and Marine Engineering, University of Michigan, Ann Arbor, Michigan 48109; perlin@engin.umich.edu
Mechanical Engineering and Applied Mechanics, University of Michigan, Ann Arbor, Michigan 48109

Key Words nonlinear surface waves, Faraday waves, standing waves, parasitic capillary waves, surface tension effects, gravity-capillary waves, vorticity, contact lines

■ **Abstract** We concentrate on the rich effects that surface tension has on free and forced surface waves for linear, nonlinear, and especially strongly nonlinear waves close to or at breaking or their limiting form. These effects are discussed in the context of standing gravity and gravity-capillary waves, Faraday waves, and parasitic capillary waves. Focus is primarily on post-1989 research. Regarding standing waves, new waveforms and the large effect that small capillarity can have are considered. Faraday waves are discussed principally with regard to viscous effects, hysteresis, and limit cycles; nonlinear waveforms of low mode numbers; contact-line effects and surfactants; breaking and subharmonics; and drop ejection. Pattern formation and chaotic and nonlinear dynamics of Faraday waves are mentioned only briefly. Gravity and gravity-capillary wave generation of parasitic capillaries and dissipation are considered at length. We conclude with our view on the direction of future research in these areas.

I. INTRODUCTION

In a recent review Dias & Kharif (1999), in their section 7, consider capillary-gravity waves in addition to gravity waves, concentrating on nonlinear effects, including those of spectra, amplitude equations, and bifurcation phenomena. Here, we wish to concentrate our discussion on the rich effects that surface tension has on free and forced surface waves for linear, nonlinear, and especially strongly nonlinear waves close to or at breaking or their limiting form. We discuss these in the context of standing gravity and gravity-capillary waves, Faraday waves, and parasitic capillary waves.

The inclusion of surface curvature (with surface tension) means that the free-surface boundary condition itself requires further boundary conditions (edge constraints). These constraints are typically contact-line conditions where the interface meets a solid surface. The contact line conditions are more formally

understood in relation to Stokes flow (Dussan 1979) but can have large dissipative effects even in an inviscid system (Hocking 1987a, Miles 1990). Indeed, contact-line dissipation effects are dominant in many containers of low viscosity fluid. The high Reynolds (Re) limit has even more complicated singular behavior at the contact line. For most water waves, there are at least three small parameters that lead to singular behavior: the slip length, nondimensional surface tension (κ), and nondimensional viscosity (1/Re). Here, we discuss contact line problems with Faraday waves primarily in the context of potential flow, and high Reynolds number viscous contact-line effects.

Surface tension also facilitates richer dynamics through altered resonance conditions. For instance, one-dimensional waves exhibit resonances when a capillary wave and a capillary-gravity wave of the same wavelength have the same phase speed. This occurs when the dimensionless surface tension κ is equal to ½, ⅓, ¼, etc. The most celebrated of these is the ripple found by Wilton (1915) at $\kappa = ½$, where the trough or the crest has a dimple formed by the first superharmonic with an amplitude that becomes one half that of the primary wave in the limit of small amplitude. For these cases, nonlinear resonances can occur for wave amplitudes $ka < 0.05$ that would otherwise be considered linear (Perlin & Ting, 1992). Hence, commonly observed wave problems with small surface-tension effects are singular in more than one way: Not only do they require the extra edge condition mentioned in the paragraph above, but they have resonances with ripples of large wavenumber N when $\kappa = 1/N \to 0$. This leads to many computational difficulties in calculating these waveforms (Huh 1991). Capillary-gravity waves also have rich instabilities leading to two-dimensional waves, as previously reviewed by Hammack & Henderson (1993).

Not only can waves of relatively small amplitude become nonlinear due to surface tension as described above, waves with large nonlinearity also exist (i.e. much steeper waves occur prior to breaking). This is seen directly by noting that the pure capillary (Crapper 1957) wave steepness limit is about five times that of a pure gravity wave (Stokes 1880, Schwartz & Fenton 1982). More importantly, small surface tension inhibits the 120° cusp of the Stokes wave and allows the wave to become much steeper.

Since interest in shorter waves is often associated with small- to medium-sized containers, wave reflection may be dominant. In the limit of large reflection, pure standing waves result, and hence it is appropriate to place a greater emphasis on standing waves for shorter waves. In general, standing waves can be obtained most cleanly by Faraday resonance (i.e. by oscillating a container vertically and hence parametrically changing the effective gravity). This Faraday wave resonance has proven to be an ideal (experimental, computational, and analytical) laboratory to study nonlinear systems, bifurcation, and pattern formation, which has created a wealth of studies largely ignored here. Contact-line effects can dominate in the low wavenumber (perhaps primary) limit, while the high wavenumber limit used in pattern formation studies necessarily creates waves dominated by capillarity.

The equations for irrotational standing waves are straightforward. In addition to the requirement that the velocity potential satisfy the Laplace equation and Neumann condition at all solid surfaces (or decay to zero at infinite depth), the inviscid flow kinematic and dynamic boundary conditions on a free surface described by $z = \xi(t)$ are

$$\frac{D\xi}{Dt} = \frac{dw^*}{dz} \tag{1}$$

and

$$\frac{D\phi}{Dt} = -y + \frac{1}{2}\left|\frac{dw}{dz}\right|^2 - \kappa \frac{x'y'' - x''y'}{(x'^2 + y'^2)^{3/2}}. \tag{2}$$

Here, $w = \phi + i\,\psi$ is the complex potential as a function of $z = x + i\,y$, * denotes the complex conjugate, and D/Dt is a material derivative. The dimensionless surface tension is given by the inverse Bond number $\kappa = k^2\sigma\,(\rho g)^{-1}$ where k is the wavenumber, t the surface tension, ρ the mass density, and g the acceleration of gravity. The damping terms are set to zero for freestanding waves (i.e. not shown in Equation 2) and are described in the next paragraph. We write the boundary conditions in this form because computational nodes are often chosen to follow material particles, especially when breaking waves are being examined (Schultz et al 1994). When κ is not equal to zero, edge constraints are required at the contact lines. The Neumann condition, $\partial\xi/\partial n = 0$, where n is the normal from the solid surface, is satisfied naturally, while special intervention is required to satisfy the pinned condition $D\xi/Dt = 0$ or a mixed condition such as that used in Hocking (1987b) or Miles (1990). Finally, for standing waves we require that the free surface elevation and potential be periodic in time and space, with symmetry conditions posed to exclude traveling waves.

Faraday (1831) forced the wave by vertical acceleration. A coordinate system fixed to the container leads to a periodic variation in gravity, so the coefficient of the first term on the right-hand side of the dynamic boundary condition (2) is replaced by $(1 + \varepsilon \sin \omega t)$. For this type of forcing, computations (and experiments!) solve an initial value problem. For the solution to become independent of the initial conditions, damping must be imposed. A simple linear Rayleigh damping (i.e. adding a term proportional to ϕ to the right-hand side of Equation 2) is usually applied, although many other possibilities can be used to model damping such as a term proportional to the second derivative of ϕ (Jiang et al 1996). These parametrically excited waves need not be periodic in time. We have seen that the addition of damping to the irrotational equations adequately predicts the correct surface profiles even for parasitic capillaries where vorticity is present.

The above description highlights many differences between free and Faraday waves. Experiments, however, require some forcing to overcome dissipation, and we have found that Faraday resonance is the best way to provide this forcing. When damping is small (water in modest- to large-scale containers), these exper-

iments match the standing wave calculations and analysis better than the sidewall forcing of Taylor (1953). We do not make a strong distinction between the two, but Faraday waves offer richer behavior because, in addition to prescribing the amplitude as is done for standing waves, one also prescribes dissipation and forcing frequency. We show that dissipation can change some of the temporal symmetries of free waves.

The inclusion of viscosity and variable surface tension gives rise to shear stresses that can drive or retard the flow. This surface tension variation can come from temperature or concentration variations. For nearly inviscid surface waves, the variation is almost always caused by surfactants that act to dampen short waves—usually considerably. This emerging topic is substantial and beyond the scope of this review. We refer to it primarily to remind the reader that care must be taken to clean the fluid as is described in the experiments discussed here. Unfortunately, detergents used to minimize contact-line effects and flow-visualization dyes and particles have surfactant-like effects.

Often capillary effects enter unintentionally through scale reduction as in towing tank ship experiments. At other times, capillary effects naturally dominate because of the small scales as in ink jet printers or in the microgravity of space. On the other hand, surface tension plays an important role in ocean spectra. It causes the Helmholtz problem describing the initial generation of ripple by wind to be well posed. Inhibiting short waves gives the appropriate wave number selection (Sobey 1986). It also can take an important role in frequency downshifting as described in Dias & Kharif (1999). Finally, longer gravity waves at or close to breaking produce short waves that are important in remote sensing, in increasing dissipation, and in affecting the fluxes at the air-water interface. Since we choose to review flows with free surfaces (avoiding wind effects) and because the frequency downshifting has been recently reviewed, for progressive longer waves we concentrate on the generation of ripples.

In this review we begin with post-1989 research. We proceed by discussing progress on standing gravity and gravity-capillary waves especially with regard to surface-tension effects. A discussion follows on several aspects of Faraday waves. Generation of and dissipation by parasitic-capillary waves is the subject of the next section. We conclude with our view of the future research direction in these areas.

II. ADVANCES ON STANDING GRAVITY AND GRAVITY-CAPILLARY WAVES

Schwartz & Fenton (1982) review the substantial literature on nonlinear water waves, including some discussion of standing waves and capillary effects. Standing waves have received far less attention because they are perceived as having only secondary importance in analyzing ocean spectra. Additionally, standing

waves are much more analytically and numerically challenging because the nonstationarity makes the inverse method (writing the complex spatial variable in terms of the complex potential) no longer possible. A temporal Fourier-series is often used, although time-marching has been found to be more successful computationally.

II.A. New Waveforms

Of course, a standing wave is sinusoidal in the linear limit, as it is just a superposition of its traveling counterpart. In this sense, other than providing possible resonances, the capillarity only serves to change the dispersion relationship. We wish to examine the strongly nonlinear limit to ascertain the limiting form of standing gravity waves and determine the effect of small capillarity on these waveforms.

Rayleigh (1915) first considered finite amplitude standing waves in two-dimensional potential flow. He neglected surface tension and finite-depth effects and calculated a power series solution to third order in the wave amplitude. Penney & Price (1952) carried a similar expansion to fifth order. Schwartz & Whitney (1981) corrected and improved to 25th order the expansion of Penney & Price. They obtained more accurate results for standing waves of relatively large amplitude in the absence of surface tension. Their expansion procedure was not capable of approaching the highest wave because the limiting wave is not the highest wave. More recent studies on standing water waves include Mercer & Roberts (1992) and Tsai & Jeng (1994).

Inspired by Stokes' (1880) analysis showing a 120° crest at the limiting form of a steady gravity wave, Penney & Price (1952) tried to find the limiting form of the gravity standing wave. The 120° crest for the traveling wave is theoretically possible, and some have been seen experimentally, if only ephemerally. Usually, the limiting wave will not be approached due to breaking, spilling, capillary wave generation, and cross-wave instabilities. However, the quest for the limiting form of the standing wave has been more controversial. Penney & Price determined that the limiting waveform would have a 90° crest. Based on this premise, they also ascertained the approximate wave height at this condition by extrapolating their expansion until an angle of $\pm 45°$ was obtained.

Several studies (for example, Taylor 1953, Mercer & Roberts 1992, Tsai & Jeng 1994) have attempted to verify these claims. Taylor (1953) found waves that approximately confirmed the height and shape predicted by Penney & Price. He also observed higher standing waves but determined that these waves were three-dimensional. Using a spectral boundary integral method combined with Newton iteration to enforce temporal periodicity, Schultz et al (1998) showed that Penney & Price (1952) overpredicted the limiting height that can be achieved without surface tension. Mercer & Roberts, using essentially the same numerical method, could have come to the same conclusion but did not. Schultz et al (1998) demonstrated that Taylor (1953) found dimensionless peak-to-peak wave heights

greater than 1.24 largely due to capillarity. The size of Taylor's experimental apparatus made capillarity very important for large amplitude waves.

There are two problems that lead to unsupported conclusions in the crest analysis of Penney & Price. The first is that temporal periodicity is not satisfied. Unlike the assumption of stationarity by Rayleigh for traveling waves, this constraint is not easily enforced. Secondly, they assume a Taylor series expansion about the crest that is not appropriate if the solution is singular. Another challenge is that this limiting form could occur when the flow momentarily becomes stationary, and hence (other than the curvature singularity if surface tension is considered) the flow singularity would be modified.

A more appropriate (but not definitive) analysis would be to determine the existence of a small time solution for various crest angles and crests. This has not been performed. The computations of Schultz et al become unreliable close to the limiting wave, and so no numerical proof is available. These computations do show, however, a very good approximation of the highest wave that is considerably smaller than that predicted by Penney & Price and seen by Taylor. The computations also infer a limiting crest angle of smaller than 90° with the possibility of a cusp (0° angle crest) formation. The wave profile comparison is shown in Figure 1 (Figure 7 of Schultz et al 1998).

Defining a standing wave profile as temporally and spatially periodic such that the free-surface elevation and velocity potential are symmetric and antisymmetric, respectively, about the peak of the wave eliminates the traveling waves and com-

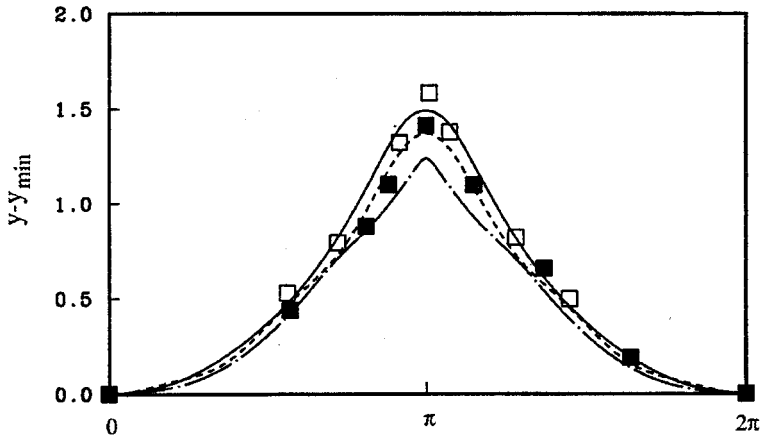

Figure 1 Comparison of peak standing wave profiles. The symbols are data from Figures 11 and 12 of Taylor (1953). The solid line is a calculated gravity-capillary wave with $\kappa = 0.0027$, corresponding to a wavelength of 32.9 cm in Taylor's experiments; the dash line is Penney & Price's 1952 gravity-wave solution at $H_{max} = y_{max} - y_{min} = 1.37$; and the dash-dot line is the highest possible gravity wave at $H_{max} = 1.2403$. (Reprinted with the permission of Cambridge University Press.)

bination standing/traveling waves of Dias & Bridges (1990). Furthermore, all nonlinear standing waves (for example, Schwartz & Whitney 1981) analyzed to date examine only the class where the kinetic energy is zero at one time during the cycle with temporal symmetry about this time. This class has nonlinear waveforms without nodes (Schwartz & Fenton 1982). This property allows computations to be performed for one half of a temporal and spatial period. However, experimental and numerical evidence (Jiang et al 1996) shows that this temporal symmetry is broken in Faraday wave systems as described in the next section.

As demonstrated in Mercer & Roberts (1992), the total energy, wave period, and wave height all reach their maxima before the formation of the sharpest wave. The limiting form is better described by the crest curvature (Schultz et al 1998) or the crest acceleration (Mercer & Roberts 1992). The limiting form is difficult to obtain computationally. An estimate of a ''crest angle'' can be obtained from the included angle given by the maximum slope on either side of the crest. The computations suggest that these angles become less than 90°.

II.B. Large Effects of Small Capillarity

The sharp crest of steep waves discussed in the last section will not appear in experiments, even for large wavelengths, because of surface tension effects. This local effect at the crest has global implications. Surface tension was first included in wave analysis/calculations by Concus (1962) and Vanden-Broeck (1984), who avoided the troubling limit of small surface tension mentioned in the introduction. Mercer & Roberts (1992) had computational difficulties adding surface tension in general. The successful introduction of large amplitude waves with small surface tension showed nonmonotonic behavior near the limiting wave as in the gravity case, but even small surface tension significantly increases the highest wave amplitude as shown in Figure 2 (Figure 6 of Schultz et al 1998). For small-amplitude waves, these surface-tension effects are diminished and linear theory is adequate. Capillarity becomes important when the wave height approaches and then exceeds the gravity-wave limit, and inhibits a possible singularity at the crest.

A laser-sheet technique (Jiang et al 1998) showed that a rounded crest and a large wave slope characterize most of the large-amplitude standing waves with large Bond numbers, demonstrating the importance of surface tension near the crest. Sometimes the protuberant crest is replaced by a flat/dimpled crest that can be thought of as a modified, highly nonlinear Wilton dimple at the crest. As long as the waves are not too close to their limiting form, the comparisons to computations are good. As the crest radius goes to zero, the crest acceleration goes to the gravitational limit, as predicted by a min-max principle first described in Schwartz & Whitney (1981).

Jiang et al (1998) found that Faraday waves (with forced vertical oscillation at approximately twice the natural frequency) produced cleaner waves than horizontal flap-type wavemakers (Taylor 1953) that change the wavelength periodically during a wave cycle and generate extra superharmonics that cause

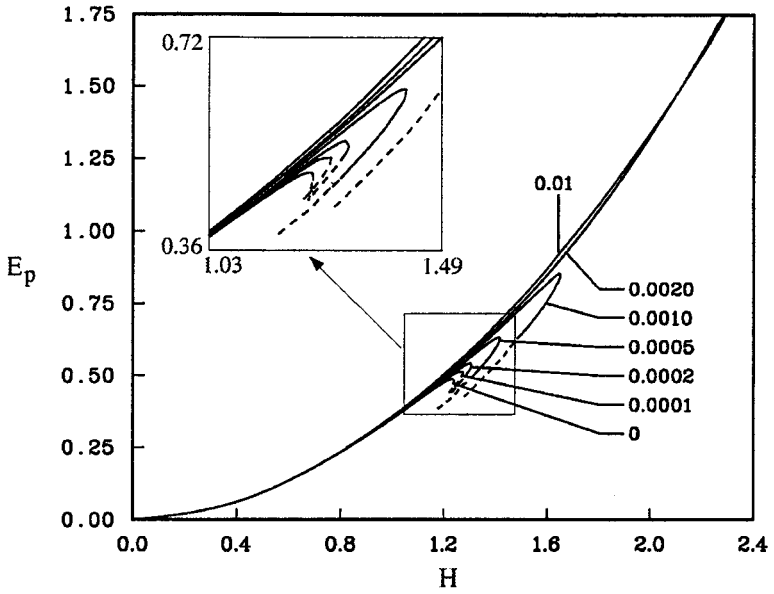

Figure 2 Potential energy versus wave height for different inverse Bond numbers, κ; the numbers refer to the value of κ for each curve. Dash lines represent results with increased errors. The inset is an enlarged portion of the curves. (Reprinted with the permission of Cambridge University Press.)

instability and irregularity in steep waves. There also appears to be more vorticity generation with this type of forcing. In moderate amplitude Faraday experiments, the wave achieved a profile with almost-zero kinetic energy (the profile changes little in a short time interval) and the maximum wave elevation at the tank center. In addition, only 16 or 32 nodes were used in most of the Schultz et al (1998) calculations to avoid resonance for small κ. Large forcing amplitude generates different waveforms as the external forcing alters the mode interaction in a standing-wave system. Overdriven Faraday waves in the Schultz et al (1998) experiments exhibited two major differences compared with the calculation of free, inviscid standing waves: temporal-symmetry breaking and ripple formation. Still higher excitation caused subharmonic temporal behavior (period tripling) and breaking.

III. PROGRESS ON FARADAY WAVES

In this section we begin where the review of Miles & Henderson (1990) concluded; we discuss the subsequent progress on Faraday waves (without reference to cross waves and edge waves). Specifically we discuss parametrically forced

standing waves in terms of surface-elevation profiles; damping and contact-line effects; breaking and drop ejection; and pattern formation. Throughout we use ''Faraday waves'' and ''parametric resonance'' (with effective gravity the parameter) synonymously.

III.A. Viscous Effects, Hysteresis, and Limit Cycles

Miles & Henderson (1990) apparently overlooked Nagata (1989), who investigated Faraday resonance in a square-based cylinder. Ignoring the effect of surface tension, using multiple scales, and following Miles (1984a), he used a Lagrangian/Hamiltonian approach and included weak linear damping in treating the Faraday wave problem while retaining the inviscid assumption. He developed coupled evolution equations at third order and discussed their stability. For the case of a slosh mode, when one half the forcing frequency is less than the natural frequency, a mixed (corner-to-corner) mode was shown to occur, while a so-called general mode occurred when one half the forcing frequency exceeded the natural frequency. This waveform is similar to the ''twist wave'' of Umeki (1991) and Decent (1997) discussed below.

Faraday waves in 2:1 internal resonance were investigated by Henderson & Miles (1991). This ratio has two distinct meanings: The forcing frequency generates a subharmonic (Faraday) wave that resonates with its own subharmonic, in which case the latter frequency is ¼ of the forcing frequency. Also, the Faraday wave resonates with its own first superharmonic, in which case the latter frequency is commensurate with the forcing frequency. Physical experiments primarily in circular cylinders measured wave amplitude over time with a single probe. Complex-demodulation estimates of growth rates and steady-state amplitudes were used to generate stability diagrams and phase space between the respective primary amplitudes. These quantities were compared to their theoretically derived counterparts. For resonance of the Faraday wave and its subharmonic, essentially all possible outcomes occurred: steady; modulated with one or two periods of the modulation; quasi-periodic; and chaotic motions. Resonating superharmonics never achieved amplitudes comparable to that of the Faraday wave. Effective damping rates taken from experiments were used where required, and the detergent Photo Flo was used in all experiments to reduce contact-line effects.

Although Milner (1991) and Miles (1993, 1994) are cited in the sub-section on pattern selection, some of the ideas they originated are required at present. Specifically these papers showed that third-order damping, and third-order damping and forcing, respectively, model important physics. In his investigation of capillary-wave pattern selection, Milner (1991) included nonlinear damping terms with Hamiltonian equations by calculating the viscous dissipation in the bulk. Miles extended the Milner formulation by including third-order forcing (which he argued is required for consistency since third-order damping was included) and finite-depth effects, and extended the results to gravity-capillary Faraday waves.

In a peripherally related paper, Generalis & Nagata (1995) included cubic-order interactions but treated a two-liquid-layer system in which one (chosen) layer is excited through Faraday resonance and the other layer through wave-wave interaction (internal to surface wave or vice versa). Their analysis is restricted to two dimensions (one surface dimension).

In a series of papers contributed in various parts by ADD Craik, SP Decent, and JGM Armitage, the authors demonstrated that including higher-order terms in the model equation partially explained measured hysteresis. In Craik & Armitage (1995), experiments were presented where the frequency was held constant while the forcing amplitude was increased until the inception of linear waves in the water-Photo Flo mixture. Then, once finite-amplitude waves were established, the forcing amplitude was decreased until the surface returned to a quiescent state. The trend in the results depended significantly on the liquid depth. The hysteresis was attributed to nonlinear damping and forcing. The evolution equation of Miles (1993) that included the effects of cubic damping and cubic forcing was shown to more accurately describe the measured hysteresis. Decent & Craik (1995) extended their model equation to include the conservative fifth-order frequency shift terms (i.e. quintic nonlinearity $\propto A|A|^4$, where A is the slowly varying complex wave amplitude) along with cubic terms in wave-amplitude for damping and forcing. Although this improved their predictions of the hysteresis observed in their experiments and others, they were still unable to describe the experimental results of Simonelli & Gollub (1989) that included waves in both surface dimensions. In a third paper, Decent & Craik (1997) exploited this same evolution equation to investigate limit cycles.

Jiang et al (1996) investigated moderate and steep Faraday waves of the fundamental mode. Here we discuss their stability measurements and their hysteresis and response diagrams. They definitively showed that contact-line effects increase the frequency (phase speed) and hence change the stability diagram in a way opposite to that usually attributed to friction. Further, they demonstrated that the addition of the wetting agent Photo Flo that reduces significantly the contact-line effects returns the stability diagram for the fundamental mode close to that obtained by the Mathieu equation for an inviscid fluid. For a small sideband-perturbation in frequency, strong modulations of the Faraday waves occurred in numerical simulations and analysis (using Rayleigh damping), and in experiments. New waveforms were reported as discussed in sections III.B and III.D. Unlike the hysteresis experiments by Henderson & Miles (1990) with fixed forcing frequency and amplitude, and quiescent initial conditions, or by Craik & Armitage (1995) with constant frequency and varying forcing amplitude, Jiang et al (1996) varied the forcing frequency in steps with fixed forcing amplitude and without returning to quiescent conditions. A soft-springlike hysteresis was demonstrated; however, beginning from the high-frequency side of the dimensionless frequency (forcing frequency divided by twice the natural frequency), the wave amplitude bypassed the jump position and increased until incipient breaking of the Faraday wave occurs. This effect was again attributed to the

contact line as the hysteresis vanished upon treating the water with the Photo Flo wetting agent and repeating the experiments. These results are reproduced in Figure 3.

Using the linearized Navier-Stokes equations for a two-layer fluid, Kumar & Tuckerman (1994) showed the system is not governed by a Mathieu equation with additional linear damping terms. This is as expected owing to the singular behavior at high Re. Their numerically generated stability map was compared to that of the inviscid solution (Mathieu equation without damping), and for the lowest tongues, they compared it also to the phenomenological model. More importantly, their good agreement with the experiments of Edwards & Fauve (1993) demonstrated that the amplitude threshold of instability is significantly different than that of the Mathieu equation with damping; however, they also showed that dispersion is only slightly affected. With less agreement, but essentially equivalent conclusions, additional comparisons were made to the experiments of Fauve et al (1992). Kumar & Tuckerman implicitly questioned many of the aforementioned results in cases other than for sufficiently weak viscosity because of an amplitude threshold issue. Kumar (1996) examined the problem of a single finite-depth fluid layer by the same method as Kumar & Tuckerman (1994). Finally, Lioubashevski et al (1997) investigated highly viscous fluids of

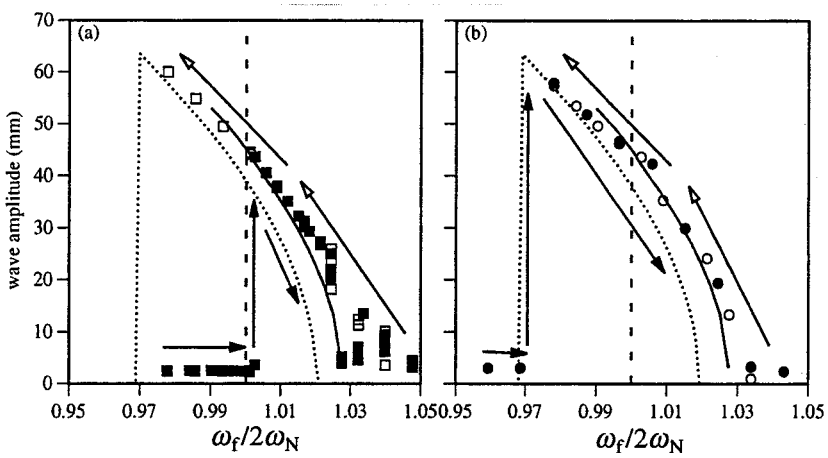

Figure 3 Wave amplitudes (Jiang et al 1996) of subharmonic resonant waves with varied forcing frequencies at a constant forcing amplitude of 2.5 mm. (a) Experiment conducted with clean water. ■ and □ represent the data measured with increasing and decreasing frequencies, respectively; – – –: our prediction using Henderson & Miles' theory (1990) with measured damping rate = 0.050 s^{-1}; ——: numerical results. (b) Experiment conducted using clean water with Photo Flo 200 in a ratio 100:1; ● and ○ represent the data measured with increasing and decreasing frequencies, respectively; – – –: our prediction using Henderson & Miles' theory (1990) with measured damping rate = 0.058 s^{-1}; ——: numerical results. (Reprinted with the permission of Cambridge University Press.)

shallow depth under parametric forcing and found similarities to the Rayleigh-Taylor instability. They discussed non dimensionalization of the problem and found that a parameter that characterizes the upward acceleration better collapses their data.

Bechhoefer et al (1995) used paraffin oil (non polar, low–surface tension fluid to reduce surface contamination) in circular and square cylinders to demonstrate that cylinders of sufficient size essentially remove the effects of lateral boundaries. They found that the Kumar & Tuckerman (1994) viscous approximation well predicts the stability threshold. They argued that a container is effectively infinite if ''the damping length of surface waves must be less than the container size.'' A stability tongue effect appears as the container size is decreased, or equivalently as the forcing frequency is decreased with fixed container size. To demonstrate that an experiment could duplicate the theoretical result that assumes infinite depth and width, we reproduce their Figure 6 as Figure 4. A circular container of depth 1.0 cm and diameter 10 cm was oscillated vertically, and the threshold acceleration for partial-surface instability (lower bound) and complete-surface instability (upper bound) are shown in the graph. The solid lines represent theoretical predictions based on Kumar & Tuckerman (1994) with temperature variation of 21° to 23°C. The dashed line is a solution to the Mathieu equation with

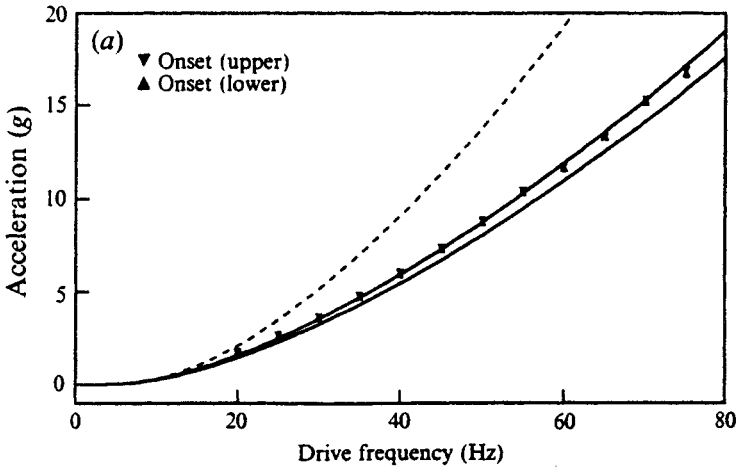

Figure 4 Instability threshold for a circular cylinder with diameter 10 cm and depth 1.0 cm (Kumar & Tuckerman 1998). Solid lines are the predictions of the model with paraffin oil at 21° and 23 °C and infinite depth and no lateral boundaries. The upper and lower thresholds are the accelerations where the entire surface and the partial surface instability occurred respectively as a function of frequency. The dashed line is the Mathieu equation prediction with phenomenological damping. (Reprinted with permission of Cambridge University Press.)

phenomenological damping $|2\nu k^2|$. However, their study is unclear how contact-line dissipation could be discounted because of sidewall wetting by the oil.

In a recent comprehensive paper, Cerda & Tirapegui (1998) investigated Faraday resonance with larger viscosity. Their discussion naturally follows that of Kumar & Tuckerman (1994), who also linearized the Navier-Stokes equations. Because numerical solutions were obtained, physical interpretation is difficult. Beginning with the linearized viscous formulation, the authors decomposed the velocity into rotational and irrotational parts and derived a governing equation for the surface elevation of each mode when lateral boundaries were neglected. As input, this equation required solving another problem for the vertical velocity of the rotational part of each mode. If viscosity were neglected, their model reduced to the Mathieu equation; however, they were unable to derive systematically linear damping. More importantly, for a highly viscous fluid (where the wave-induced fluid motion is viscous throughout) the authors determined a model that reduced to a Mathieu equation when truncated beyond the first two terms of an infinite-term series. This equation is similar to one they obtained phenomenologically for deep water and weak viscosity, except with different coefficients. $\ddot{\xi}_k(t) + 2\bar{\gamma}_k \dot{\xi}_k(t) + \bar{\omega}_k^2 (1 + \Gamma_k \cos\Omega t)\xi_k(t) = 0$. ξ_k is the complex wave amplitude, $\bar{\gamma}_k$ and $\bar{\omega}_k$ are altered damping coefficient and frequency, respectively. The authors transformed this equation to a linear Schrödinger equation that they then solved approximately using the WKB method. Cerda & Tirapegui compared their solution to the experiments by Edwards in Kumar (1996) and Kumar & Tuckerman (1994). They give a very lucid physical explanation of the instability threshold as compared to the Rayleigh-Taylor instability (cf Lioubashevski et al 1997).

The seminal experiments by Wu et al (1984) demonstrated the existence of a standing soliton excited by parametric resonance (i.e. a particular Faraday wave). Subsequent theoretical contributions by Larraza & Putterman (1984) and Miles (1984b) increased knowledge in this area greatly. We adapt the definition used by Miles & Henderson (1990) that a Faraday wave is a parametrically excited wave, while a cross wave is a wave with crests normal to a moving boundary, i.e. a wavemaker. We do not examine cross waves defined in this manner; however, as some authors have used the term cross wave in the context of Faraday waves to designate the wave in the transverse (narrow-width) direction, we do include a brief discussion of them. The cubic Schrödinger equation derived by Miles (1984b) for parametric excitation was re-examined by Laedke & Spatschek (1991), especially with regard to its stability. A new instability regime was found and confirmed numerically, and stable regimes for solitary waves were also shown to exist. Guthart & Wu (1991) used a multiple-scales analysis to derive a cubic Schrödinger equation equivalent to that of Larraza & Putterman (1984) when the forcing amplitude was set to zero. It was shown also to be reducible to the equation of Benjamin & Ursell (1954). For particular choices of coefficients another solitary-wave solution to the governing equation was determined with *tanh*-

dependence, rather than the *sech*-dependence in Miles (1984b). Guthart & Wu stated that preliminary experiments confirmed its existence. Umeki (1991) examined Faraday waves in two surface dimensions using an average Lagrangian formulation derived by Umeki & Kambe (1989). This study extended Miles (1984a) by the inclusion of capillary effects. Homoclinic chaos for 2:1:1 external-internal resonance was demonstrated.

Wang & Wei (1994) presented evidence that parametrically excited, paired standing solitons attract-collide-repel each other and thus can be separated by a symmetrically placed wall. Moreover, this suggested that a single soliton's interaction with a wall boundary should be equivalent to a soliton interacting with its mirror image, and this was demonstrated experimentally. Chen & Wei (1994) investigated the behavior of a standing soliton generated by parametrically excited resonance with modulation. They purposely added slow-time scale modulation to their experiments and compared its effect to inverse-scattering perturbation theory. Phase portraits and Poincaré maps of several limit cycles were presented showing the existence of a strange attractor. They conducted experiments with a water-soap mixture that confirmed the theory for the parameter range as long as experimentally determined damping rates were used. Friedel et al (1995) focused on the nonlinear transitions between the four regions of the stability diagram for the standing soliton solution of Faraday resonance. They showed that a common thread existed between several published papers predicting a period-doubling route to chaos for so-called long systems. Using a weakly nonlinear theory, now for deep water, Decent (1997) derived yet another cubic Schrödinger evolution equation with damping and forcing terms retained to third order in wave amplitude, and he found additional time-modulated, non–constant phase, or co-existing constant phase solitary waves. These results are not surprising but clearly demonstrate the need to include higher-order terms. Furthermore, he presented one route to the three-dimensional twisting waves investigated by Umeki (1991) and showed its plausibility by demonstrating that the cross-tank sloshing mode is unstable to three-dimensional twisting waves.

In completing this section, we mention a paper by Bechhoefer & Johnson (1996) studying periodic, triangular-displacement forcing. They investigated stability tongues that are reproduced here in Figure 5 for the Mathieu equation triangularly forced (by sequences of delta functions), one of which represented asymmetric forcing. γ represents damping, Δt is the period of the forcing, T represents the period of the natural wave, and r is $\Delta t_2/\Delta t$ with Δt_2 related to the time when the forcing is applied. Additionally, they used the analysis of Kumar & Tuckerman (1994) for a viscous fluid to investigate triangular forcing. The linear stability analysis was simplified greatly using triangular forcing.

III.B. Nonlinear Waveforms of Low Mode Numbers

In discussing Faraday waves, it is easiest (a relatively simple measurement typically made with a probe) to consider the surface elevation at a point. There has been less interest in the parametric wave excitation wave profile for low mode

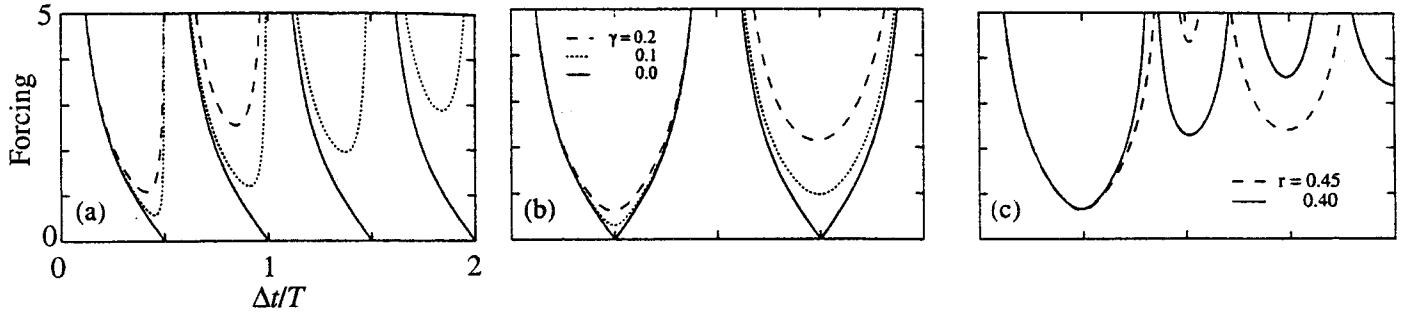

Figure 5 Resonance tongues for the Mathieu equation (Bechhoefer & Johnson, 1996) driven by a periodic sequence of delta functions for various damping, $\gamma = 0.0$, 0.1, and 0.2. (a) Delta functions of equal sign, (b) Delta functions of alternating signs, (c) Delta functions derived from an asymmetric triangle wave for $\gamma = 0.2$ and different values of r. (Reproduced with permission.)

numbers as compared to high wave modes and their patterns discussed below. However, the profile shape is important as steep slopes lead to breaking, aerosol formation, and increased remote-sensing radar backscatter of the ocean surface. In addition, the steep surface slopes can be important and useful in microgravity applications, for example in wicking flows. As the waveform of a soliton is of particular interest, and their stability is discussed in section III.A., they are disregarded here.

To reduce contact-line effects, Henderson & Miles (1991) conducted experiments with Photo Flo. They investigated hysteresis, stability, phase space, and resonance between various modes using a wave probe to measure amplitudes. Wave slopes at breaking were reported also as calculated from the measured amplitudes. Spatial information was not recorded in their experiments. The probes were located at a point of maximum surface displacement that oftentimes was at the center of the cylinders. That same year Guthart & Wu (1991) published theoretical results of a soliton-like twist wave, and they mentioned substantiating experiments, but to our knowledge these results were never published.

Recently, Jiang et al (1996, 1998) measured surface-elevation profiles of the fundamental mode, defined as one wavelength in their large-aspect ratio (length-to-width) container. Although periodic, the waves were asymmetric in time because of dissipation in the physical experiments and in the numerical simulations modeled with Rayleigh damping. Spatial symmetry was invariably present. Interestingly, once the waves became strongly nonlinear owing to increased forcing, the profile shapes during decreasing elevation at the tank center had *flat* crests that evolved from a maximum surface elevation with a dimpled crest. The surface elevation during increasing wave elevation at the centerline of the container exhibited more expected behavior although higher spatial harmonics were evident; however, immediately after the profile reached its maximum elevation at tank center, the dimple formed. A surface-detection algorithm was implemented to determine the profiles presented in Figure 6. Further increases in forcing produced two plunging breakers, one to each side when the crest was at midtank,

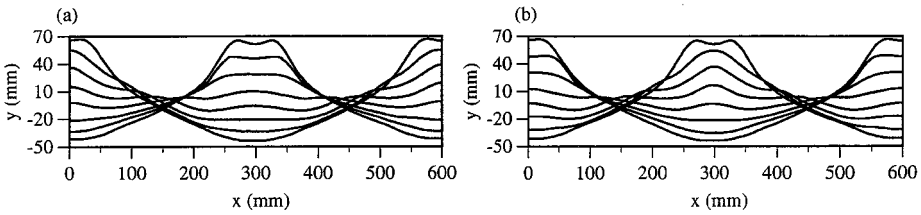

Figure 6 Faraday wave profiles obtained from laser-sheet imaging for a 3.23 Hz oscillation with a forcing amplitude of 3.85 mm. (a) Surface-detected experimental profiles during decreasing surface elevation at the centerline. (b) Surface-detected experimental profiles during increasing surface elevation at the centerline. (Reprinted with the permission of Cambridge University Press.)

and one on each end-wall one-half wave period later. This newly discovered waveform and its breaking counterpart represent one manner in which Faraday waves steepen and eventually break.

III.C. Contact-Line Effects and Surfactants

Miles (1991) used a complex-valued boundary condition (i.e. a slip-length) along the lateral boundaries to allow a phase shift between the free surface and the container boundary, and he investigated the free-surface oscillations of an inviscid fluid. We envision his formulation and solution analogous to a spring-mass-damper system where the contact line always resists motion (due to capillary hysteresis) as suggested by Miles in 1967. Miles' primary result was an expression for the frequency change compared to the natural (inviscid, 90° contact angle) frequency of the system. Henderson & Miles (1994) conducted experiments with brimful deep-water conditions in a circular cylinder with clean and with fully contaminated (inextensible) water. They found good agreement between Miles' theory and their increased experimental frequency. The damping rates, however, do not agree. Since the container was brimful (i.e. it has a pinned contact line), contact-line damping was excluded partially in their experiments. Still, they were unable to explain the larger damping rates measured in their experiments.

Milner (1991) provided estimates of dissipation at the moving contact line by assessing the work done by surface tension as the contact-line position and angle change. His motivation was to account for this dissipation relative to that in the bulk as it was not included in his analysis. Christiansen et al (1995) used the estimate provided by Milner to demonstrate that inclusion of the moving contact-line dissipation was required (in addition to the bulk dissipation) to obtain reasonable damping estimates. Furthermore, the free parameter, s, a necessary length scale suggested to be 10^{-7} cm by Milner, required values for ethanol of 10^{-6} and for propanol of 10^{-5} cm for good agreement with the experimental data.

Using a large aspect ratio (tank length to width) of 10:1 and deep water, Faraday-wave experiments and numerical estimates of Jiang et al (1996) also found that damping rates were much larger than those predicted by theory without contact-line contributions. Unlike the experiments of Henderson & Miles (1994) with pinned contact lines, and those of Christiansen et al (1995) for higher frequencies (50–500 Hz), these experiments focused on the fundamental mode, i.e. one wavelength, in a 60-cm-long channel. Although the contact line was not pinned by design, its effect on the dynamics was important. With treated water (i.e. particulate filtered to 0.2 microns, carbon adsorbed, and de-ionized), the subharmonic viscous natural frequency was greater than the inviscid natural frequency as was the case for Henderson & Miles (1994), and this effect was shown to be attributable to increased phase speed as originally demonstrated by Benjamin & Scott (1979) for pinned conditions. To demonstrate the effect on phase speed, Jiang et al (1996) presented results for an aspect ratio of 2.61:1 as well as for Photo Flo-treated water. Both reduce contact-line effects without pinning the

contact line, yet dramatically shifted the viscous frequency closer to theoretical predictions of the inviscid natural frequency.

To determine the effect of a static contact angle on Faraday waves, Henderson et al (1992) conducted experiments with acute, near $\pi/2$ rad, and obtuse static angles (i.e. hydrophilic, neutral, and hydrophobic surfaces). They found that damping rates decrease with increasing contact angle, while frequencies increase with increasing contact angle. By prescribing an infinite slope of the meniscus at the wall—a zero contact angle wetting fluid, Miles (1992) avoided capillary hysteresis. For standing waves in a deep circular (and rectangular) cylinder, he showed that the frequency reduction was larger than that due to capillary energy and hence helped explain experiments by Cocciaro et al. (1991) that used horizontal excitation rather than Faraday-wave excitation.

In a study of Faraday-wave damping in slightly viscous fluids, Martel & Knobloch (1997) demonstrated that viscous modes (i.e. bulk motion) can decay slower than gravity-capillary waves, and they therefore should be included in weakly nonlinear theory. In other words, second-order decay-rate corrections are necessary to determine damping rates comparable to those measured experimentally. Comparison of their theoretical damping predictions, i.e. their exact solution compared to their first-order and second-order approximations for realistic Reynolds number, indicate that second-order corrections are required. They speculate that Henderson & Miles' (1994) not including the second-order damping correction is likely the cause of the discrepancy between measured and predicted damping values as the viscous modes and gravity-capillary modes contribute comparably. The same concept was treated comprehensively in a subsequent paper by Martel et al (1998). They successfully ignored capillary hysteresis by using a brimful container and made a first correction to the Stokes boundary layer to include bulk viscosity. Comparison to Henderson & Miles (1994) experimental damping rates showed significant improvement.

III.D. Breaking and Subharmonic Waves

Henderson & Miles (1991) measured the stability space for subharmonic resonance in a circular cylinder where breaking and other regions were delineated. They defined breaking by surface ejected drops of water so that their assessment would be objective; however they did not investigate this phenomenon further. This definition discounts plunging or spilling waves. A linear relation was found between the surface slope (that was not measured directly, but was calculated from the measured amplitude and the wavenumber) and the tuning parameter (i.e. a non-dimensional frequency difference). It was clear that the subharmonic resonance affected the breaking criterion, as they had previously measured larger steepness with no breaking when only one mode was present. They also noted that the breaking was associated with a quasi-steady (not chaotic) state.

In the first of several publications regarding Faraday waves, Jiang et al (1996) reported a new form of steep standing wave with a symmetric double-peaked

(dimpled) crest that appeared at steepness far less than limiting standing waves, and at a surface tension less than for Wilton ripple resonance. For these rectangular-planform containers, flat crests were observed at slightly smaller forcing as well as during the cycle in which dimpled crests appeared. Slightly increased forcing caused wave breaking as shown in Figure 7 (Figure 1 of Jiang et al 1998), the stability space with p and q the dimensionless detuning parameter ($p = 4\omega_i^2/\omega_f^2$) and forcing parameter ($q = 2Fk_i \tanh k_i h$), respectively. They ω_i and ω_f are wave frequency and forcing frequency, whereas F and h are the forcing amplitude and water depth, respectively. The incipient breaking steepness ($H\lambda^{-1}$, wave height to wavelength ratio) of 0.216 supports the conclusion that surface tension facilitates steeper standing waves. Initially, breaking occurs by symmetric-in-space plungers to each side of the centerline, and with a half-period lag at each end of the channel. To further investigate the breaking process, Jiang et al (1998) studied two-dimensional steep and breaking waves, again in a 10:1 aspect ratio rectangular container that was 60 cm long. They were able to estimate the breaking energy dissipation due to the periodicity (even with breaking). By increased forcing, the waveform evolved from a dimple-crested wave, which was shown to be the result of interaction between the first and second temporal harmonics, to two crest-symmetric, mild plunging breakers; to period-tripled breaking subharmonic standing waves. In the period-tripled breaking waves, the three waveforms have different mode shapes, one of which was not previously evident. The three sequential modes observed were a sharp crest ($<30°$) with an upward jet and large plunger that reenters the surface to either side, a flat or dimpled crest with mild plunging breakers to each side, and a rounded smooth crest exhibiting no breaking. These modes are shown schematically in Figure 8 (Figure 7 of Jiang et al

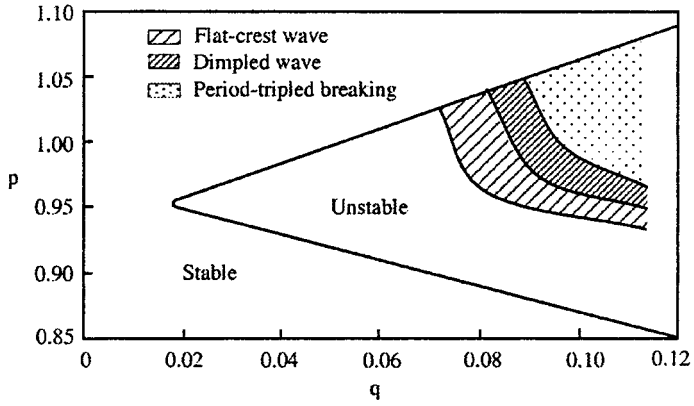

Figure 7 Locations in parameter space of the various waveforms in Faraday-wave experiments of Jiang et al (1996). The solid line represents the neutral-stability curve measured from experiments where p and q are the nondimensional forcing frequency and amplitude. (Reprinted with permission of Cambridge University Press.)

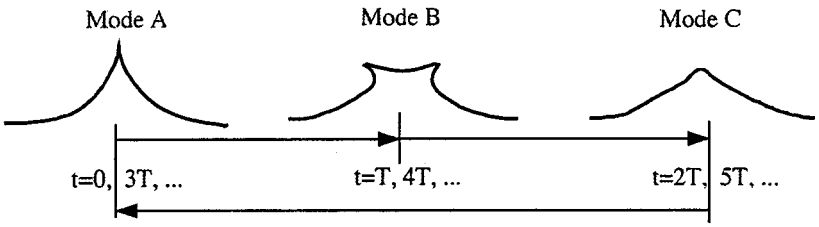

Figure 8 Schematic of three different modes during period-tripled breaking. *T* is the temporal wave period prior to period tripling (i.e. twice the forcing period). Each crest feature is observed at the tank endwalls 1.5*T* after it is observed at the tank centerline. (Reprinted with permission of Cambridge University Press.)

1998). With sufficient forcing, the period tripling was observed at all forcing frequencies near the linear natural frequency. The period tripling was observed to manifest itself in the amplitude spectrum at frequencies of $f/3$ with f the subharmonic wave frequency; see Figure 9 (Figure 13 of Jiang et al 1998). The dissipation rate was determined from forcing measurements, and for the observed frequencies breaking energy dissipation was approximately 5% of the total wave energy per temporal period; this energy was comparable to all other dissipation mechanisms present. Although period tripling was noticed only after breaking, hindsight uncovered that the frequencies apparent in the postbreaking amplitude spectrum were present in the nonbreaking, but steep waveforms. Their analysis was not able to confirm the period tripling as it occurred only for amplitudes when the numerics became suspect. The mechanism responsible for the period tripling remains unknown.

III.E. Drop Ejection

Goodridge et al (1996) experiments on Faraday waves increased the forcing until drops were ejected from the surface, and then they decreased the forcing until the threshold of incipient droplet ejection was determined. Three fluid mixtures were investigated: water, ethanol, and water-glycerin solutions. The ejection of fluid from their circular cylinders was a function of the frequency and the surface tension, and the manner in which fluid was expelled differed for the lower frequency forcing (high frequency gravity waves) versus the higher frequency forcing (low frequency capillary waves). For gravity waves, surface tension becomes locally important (see Section II.B.) and a Rayleigh capillary instability occurs at the crest as do random droplet ejections. A dimensionally grounded expression based on frequency and surface tension yielded reasonable agreement with experiments except at the lowest frequencies. Disagreement was attributed to viscous effects, and hence their subsequent study (Goodridge et al 1997) included viscosity variation along with frequency and surface tension. Drop ejection for low viscosity fluids was found to depend on frequency and surface tension, while for

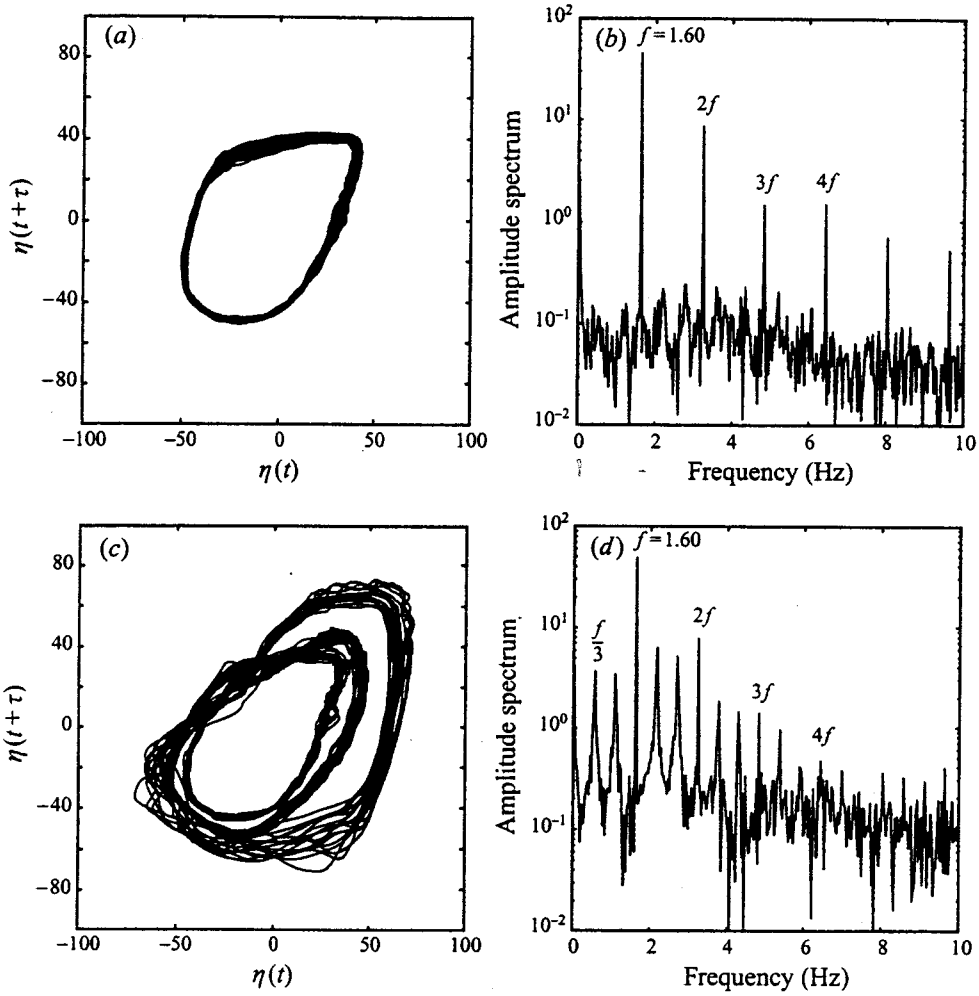

Figure 9 (a) Phase diagram and (b) amplitude spectrum for the surface elevation at the tank center. Wave is nonbreaking but steep (forcing frequency 1.60 Hz, forcing amplitude 4.15 mm). (c) and (d) are the same for period-tripled breaking (forcing frequency 1.60 Hz, forcing amplitude 4.57 mm). (Reprinted with permission of Cambridge University Press.)

high viscosity fluids, viscosity replaced surface tension as the second important variable. Goodridge et al (1999) conducted and analyzed another set of droplet ejection experiments in the high-frequency range (i.e. where capillary effects dominate gravitational effects or equivalently large κ). The ejection rate was well-predicted by a power law once the acceleration was scaled by its acceleration ejection threshold. The ejection rate was also well predicted by integrating the probability function of wave height (scaled by its root-mean square value) above

a breaking threshold based on a steepness criterion. Lastly, Goodridge et al (1999) demonstrated that the interarrival time between ejections was Poisson distributed. This led to the conclusion that the ejections are uncorrelated random occurrences.

In a narrow channel with deep water, Jiang et al (1998) observed Rayleigh instability and drop formation from the wave crest similar to the lower frequency observations by Goodridge et al (1996). The aspect-ratio constraint preserved a predominantly one-dimensional surface to incipient breaking. Mode A of their period-tripled breaking standing waves exhibited the drop formation as follows: Water is ejected at the maximum crest elevation and forms columnar drops; the jet subsequently impinges on the free surface forming a depression followed by a rebounding jet and entrained air. The motion remains essentially two-dimensional until jet/crest breakup. At times the crest exhibits asymmetry (leaning to one side) and subsequently impinges on the corresponding side of the surface.

Smith et al (1998) constructed a simple model and conducted a set of experiments to investigate droplet ejection/atomization from a sessile drop on a piezoelectric driven vibrating plate. The circularly clamped diaphragm responds at its lowest mode, generating an axisymmetric gravitational field varying with position as well as time, unlike the usual Faraday forcing. By increasing the forcing amplitude until the Faraday waves developed incipient drop ejection, and allowing time for the system to evolve further, they witnessed a gradual increase in drop ejection until a bursting event where the droplet literally exploded into spray. The phenomenon was modeled by assuming nonlinear spring and damper, and a simplified effective gravitational field that varies in time. The simple idealization captured some of the important physics qualitatively.

III.F. Pattern Formation (High Mode Numbers) and Related Topics

In reading the abundant literature on pattern formation, it becomes evident that the problem remains unsolved. Yoshimatsu & Funakoshi (1998), for example, in their section 4 make it clear that results depend on the assumptions made and the order of the approximation, and although that is usually the case, here seemingly any pattern can be found (i.e. stripe, square, roll, hexagon, 8-fold quasipattern, mixed symmetry 6/8, 10-fold quasipatterns, etc). Hence, we present several references but do not discuss them. These references include Douady (1990), Milner (1991), Mesquita et al (1992), Miles (1993), Bosch & van de Water (1993), Edwards & Fauve (1994), Bosch et al (1994), Miles (1994), Christiansen et al (1995), Feng & Wiggins (1995), Binks & van de Water (1997), Binks et al (1997), Zhang & Viñals (1997), Yoshimatsu & Funakoshi (1998).

III.G. Chaotic and Nonlinear Dynamics

We choose not to discuss chaotic and nonlinear dynamics in detail for brevity, but we include several references for completeness. These topics include manifolds, chaos, symmetries, bifurcations, breathers, and kinks, for example. Some

of the attendant references are: Simonelli & Gollub (1989), Crawford et al (1990), Dias & Bridges (1990), Crawford (1991), Crawford et al (1993), Landsberg & Knobloch (1993), Chossat & Dias (1995), and Landsberg & Knobloch (1996).

IV. DEVELOPMENTS REGARDING PARASITIC CAPILLARY WAVES AND ASSOCIATED INSTABILITIES

In this section we discuss a very important progressive-gravity-wave phenomenon that necessarily includes surface tension as the underlying wave crest steepens. Increased use of remote-sensing on geophysical scales where surface hydrodynamics understanding and input is germane requires further study of these short waves. Likewise, the cause and evolution to breaking is related to this small-scale phenomenon, as is the dissipation process. First reported in Cox (1958) in his investigation of wind-driven laboratory waves, the presence of ripples on the front face of underlying gravity and gravity-capillary waves has been the subject of several subsequent investigations. The seminal theoretical breakthrough and process clarification by Longuet-Higgins (1963) demonstrated that the increased curvature at the crest of a steepening gravity wave generated ripples upstream of the crest as well as longer waves downstream. Several studies followed this important contribution; however, we begin our discussion with research appearing after 1990.

The quasi-potential formulation of Ruvinsky et al (1991) included a viscous term proportional to the vertical gradient of the vertical velocity component that was an outgrowth of the linearization of the vorticity transport equation and subsequent simplification. The motivation for improving the theoretical/numerical approximation to the parasitic-capillary-generation process was that experiments exhibited ripples at significantly lower steepness underlying waves than accorded with any theory. In addition, the experimental ripple wavetrains maintained their wavelengths as their steepness increased. They found qualitative agreement between their numerical predictions of the steepness and wavelength of the ripples versus those observed in experiments. Perlin et al (1993) experiments on underlying waves with frequencies of about 5 Hz used vertical exaggeration and high-speed video to observe parasitic capillaries in time and space for the first time. Comparisons were made to the theories of Longuet-Higgins (1963), Crapper (1970), and Schwartz & Vanden-Broeck (1979). Significant differences were found: The experimental parasitic capillaries were larger than those predicted by Longuet-Higgins theory when the measured underlying-wave steepness and phase speed were used, and the experiments exhibited smaller wavenumbers than the theoretical prediction. Crapper's theory predicts reasonable amplitudes on the forward face of the underlying wave, but overly predicts amplitudes on the rear face compared to the experiments. Schwartz & Vanden-Broeck theory assumes symmetry about the crest and trough and predicts significantly smaller amplitudes than observed. A satisfactory theoretical/numerical explanation of the measured

profiles was not published until Jiang et al (1999), discussed below. Longuet-Higgins (1995) improved his previous effort in two ways: The wave profile of the underlying wave was updated and improved, providing a better crest curvature than used earlier, and the particle accelerations determined were applied in determining the dynamics of the parasitic capillaries. Periodic space and time assumptions were retained, however. A critical wave steepness dependent on wavelength was determined, above which the flow was termed supercritical, below was termed subcritical. Subcritical conditions permit the capillary wave to be generated along the entire surface, and their energy to propagate to all surface locations. Supercritical waves can exist only in the underlying trough and are blocked from the crest. Longuet-Higgins (1995) demonstrated satisfactory agreement between theory and experiments by Cox (1958), Ebuchi et al (1987), and Perlin et al (1993) (although his concerns about the experiments were not warranted, as is demonstrated below). Debiane & Kharif (1996) included surface tension in their formulation and discovered a new family of limiting profiles of steady gravity waves that includes two trapped bubbles, one to each side of the crest. As is the case for standing waves, they demonstrated that the steepest progressive wave exceeds that of the steepest gravity wave.

Using a Hamiltonian formulation that included damping by coupling their wave system to a heat bath source/sink, Watson & Buchsbaum (1996) investigated several capillary wave–longer wave interactions including the radiation of parasitic capillary waves. Unlike the Longuet-Higgins (1995) treatment that used a quasi-stationary assumption, they started with a Stokes wave and let the system evolve in time. They calculated surface profiles that exhibited millimeter waves on the forward face, and centimeter waves near the crest. Unfortunately, no direct comparisons were made between parasitic-capillary generation and other theoretical treatments or experiments.

In the interest of tractability, researchers analyze spatially and/or temporally periodic flows. Important and useful information may be gleaned from these solutions; however, problems may be oversimplified, and the results may not be reproducible in experiments. Ripple generation on steep gravity-capillary waves is one example where unsteadiness needs to be included as shown in Jiang et al (1999). It was shown in Perlin et al (1993) that parasitic capillaries remain essentially phase-locked with the underlying wave while spatial amplitude modulation occurs. Perlin et al also demonstrated that the ripples were significantly steeper than the theory of Longuet-Higgins (1963). Longuet-Higgins (1995) incorrectly stated that some disagreement was due to free wave ripples experimentally generated by the plunger wavemaker that hence were not parasitic capillary ripples. Additional experiments with flap-type wavemaker (to remove the possibility of any pumping effect) and numerical simulations presented in Jiang et al (1999) using the Cauchy integral method corroborate completely the experiments in Perlin et al (1993) as well as clarifying other important physics. Jiang et al (1999) demonstrated that the underlying gravity-capillary waves, with finite initial perturbation, exhibit a ''pitching'' crest motion and alternating asymmetry in wave

slope. Figure 10 (their Figure 9) shows the profiles for 6.5-cm waves with a sinusoidal initial condition and $ka = 0.15$. The wave moves from left to right in laboratory coordinates. The first four wave cycles are shown in a coordinate moving with the linear phase speed. Initially the crest tilts forward and ripples are generated on the forward face. After two wave periods, the crest starts shifting backward (30th profile from the top), a new crest emerges from the first ripple on the forward face as if the crest is ''shifting'' forward. The parasitic capillaries eventually reach the rear face of the next crest. This ripple generation process differs significantly from previous experimental studies where only forward-tilting crests were observed. The underlying wave crest and the first ripple interaction persist for long time calculations also. The alternating crest asymmetry is causing the changes in the parasitic capillaries, not the blocking effect of the steep underlying wave as suggested in Longuet-Higgins (1995). The crest-ripple interaction is reduced when third-order gravity-capillary waves are used for initial conditions. The maximum crest elevation, however, does shift between two posi-

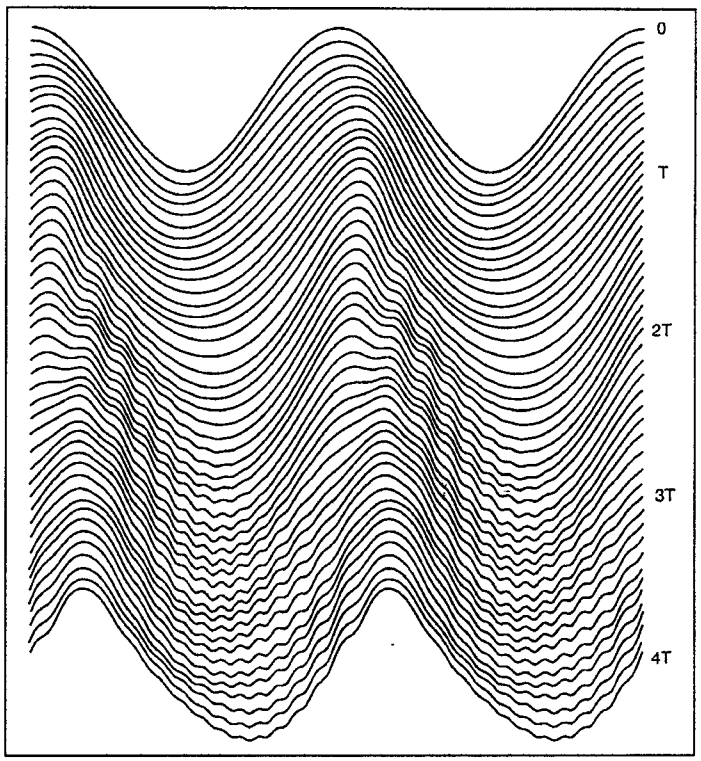

Figure 10 Simulated 6.5-cm wave in coordinates translating at the linear phase speed, left to right. The wave steepness is 0.15 while the Reynolds number is 3294. The vertical scale is exaggerated. (Reprinted with the permission of Cambridge University Press.)

tions at the edge of the crest in later stages. Significant ripples are observed in the wave trough as in the steady solution of Schwartz & Vanden-Broeck (1979). The experiments exhibited crest-shifting motion very similar to that shown in Figure 10.

Several recent papers study the existence and structure of a high vorticity region in the crest of the underlying gravity-capillary wave. The discussion was precipitated by Longuet-Higgins (1992), who estimated the vorticity shed by a train of parasitic capillaries and stated that it may contribute to the vorticity in the roller at the crest of the underlying longer wave. Mui & Dommermuth (1995) constructed a two-dimensional model to calculate, among other things, the vortical structure beneath parasitic capillaries. For steep waves, they showed that the vorticity shed from the parasitic capillaries generated by a 5-cm underlying wave causes a surface current equal to 25% of the phase speed of the system. As expected, calculations confirmed the presence of highly vortical regions on the rear face of the capillaries and that dissipation is greatly enhanced by the capillaries' existence. Flow separation was seen numerically for very steep capillaries. However, no evidence of a surface roller was observed in the crest of the underlying wave. (Below we present a vorticity calculation from Mui & Dommermuth and an experiment from Lin & Perlin (1998) that agree qualitatively, and neither of which have an organized roller at the underlying gravity-capillary wave crest.) Further, the ripple generation is predicted by the irrotational model of Jiang et al is essentially irrotational. The crest-roller issue remains largely unresolved for steep gravity-capillary–parasitic capillaries wave systems in the absence of wind.

Longuet-Higgins (1996) discussed capillary jumps on irrotational flows due to steady currents and showed that when the horizontal current decreases from a magnitude greater than the minimum phase speed of a linear gravity-capillary wave to less than the minimum phase speed, these jumps are expected. He demonstrated that the forward face of a gravity wave can provide the necessary conditions for such a jump and that parasitic capillaries are generated when the jump leaks energy down the forward face.

An experimental result from Lin & Perlin (1998) is presented in Figure 11 along with a numerical simulation from Mui & Dommermuth (1995), both for a 5-cm long underlying wave, though the latter wave was significantly steeper. (To retain two-dimensionality in the experiments, restrictions on steepness were required.) The waves travelled left to right, and the vertical exaggeration differs in the figures. (We have reversed horizontally the figure axis that originally appeared in Mui & Dommermuth.) The similarities are striking. Positive vorticity is defined as clockwise, with organized clockwise vorticity shown in the troughs of the parasitic capillaries (by the arrows in Figure 11a, see color insert), and counterclockwise vorticity just upwave (in the crests of the parasitic waves). However, neither figure exhibits organized strong vorticity (i.e. a roller) in the primary wave crest as predicted by Longuet-Higgins (1992), for a slightly longer wave.

Several investigations regarding the (crest) instabilities of gravity waves and the related problem of breaking progressive waves and the attendant parasitic capillaries generated during the breaking process have been undertaken, and consequently these efforts are discussed. Longuet-Higgins & Cleaver (1994) find an instability of the gravity wave crest, and hence the Stokes limiting waveform cannot be achieved. In so doing, it is conjectured that the source of parasitic capillaries may be not the crest curvature itself, but the toe of the instability. Banner & Peregrine's (1993) review of wave breaking in deep water shows that numerical and experimental breaking heights fall far short of the limiting form of a Stokes wave. The numerical and experimental breaking criteria of Schultz et al (1994) depend strongly on the wave history and hence show that breaking is more an unsteady process than a result of a local instability. [A wavetrain instability of the Benjamin-Feir type may lead to local wave growth and breaking (Tulin & Li 1991).] Well before breaking, the computations of Schultz et al (1994) exhibit singularity formation on the forward face of a gravity wave. This singularity may contribute to capillary ripple production.

Spilling breaker experiments of Duncan et al (1994) compare well to the theory of Longuet-Higgins & Cleaver, and Duncan et al further discovered that the unstable bulge itself develops large-amplitude disturbances and attributed them to instabilities on a shear layer (between the bulge moving down the forward face and the underlying flow). To explain these latter instabilities, Longuet-Higgins (1994) demonstrated the likelihood that they are due to vorticity shed from parasitic capillaries that are created as a result of the toe of the bulge and exist downwave. In an investigation of plunging deep-water waves, Perlin et al (1996) recorded the existence of parasitic capillaries beneath the overhanging jet of a plunger, where there is also a sharp change in the surface shape (i.e. a toe). In a revision of one result from Longuet-Higgins & Cleaver (1994) (i.e. that only one unstable mode existed), Longuet-Higgins & Dommermuth (1997) demonstrated the existence of multiple unstable modes. Additional investigation reported in Longuet-Higgins & Tanaka (1997) has shown that superharmonic instability is indeed focused in the crest region as initially suggested by Longuet-Higgins & Cleaver (1994); however, surface tension was not included in their analysis.

Spectral formulations of capillary waves on longer waves are also of interest. Although it was argued by Longuet-Higgins (1992) that wave interactions are more important than wind in the generation process of parasitic capillaries, parasitic capillaries are also an important process on steep gravity, and gravity-capillary waves (of proper wavelength) generated by wind. We do not provide a comprehensive discussion of wind-wave spectral formulations, for which there is an abundant literature. Rather, we mention articles that discuss parasitic capillaries in the presence of wind. Watson & McBride (1993) formulated a model that included many of the important mechanisms responsible for the generation of capillary waves by longer waves for low-wind speeds (to avoid wave breaking and wind-driven currents). In agreement with Longuet-Higgins' conclusion, they found that low wind is not a major contributor to the shortest capillary waves.

Zhang (1995) reported experiments in a wind-wave facility for wind speeds of 5 to 10 ms^{-1}. Relevant to parasitic ripples, qualitative observations showed that the steepest, longest capillary appears crest adjacent on the forward face and that the wavelengths and slopes decrease along the forward face toward the trough. Quantitatively the longest ripple was about one cm, and more characteristically about 0.6 to 0.7 cm. As one would expect, Zhang saw that the inherently two-dimensional wind-generated underlying waves had a direct effect on the ripples' directionality. In addition, even when the underlying waves had a one-dimensional surface structure, the parasitic ripples exhibited longitudinal modulations, as was shown previously in the case of freely propagating capillary-gravity waves of similar wavelengths by Perlin & Hammack (1991).

Fedorov & Melville (1998) numerically examined nonlinear parasitic-capillary waves by using a cosine pressure distribution to model simplified wind forcing and to balance viscous dissipation. Pressure and underlying wave steepness were chosen such that the waves were periodic in time and space (i.e. balanced) and could be rendered steady by a Galilean transformation. The authors state that it is necessary to include the effects of parasitic capillaries in any comprehensive treatment of wind-wave generation. A boundary-layer formulation, a correction to the lowest order irrotational problem, was used. Wave steepness and pressure amplitude were treated as independent parameters. Two classes of solution were found for weak pressure forcing: one that resembles the Miles' mechanism of wave generation (i.e. pressure forcing) with maximum surface pressure near the trough, and one that is in accord with a shear-flow instability with maximum surface pressure near the crest. Several important conclusions were made including damping enhancement of the longer waves by one to two orders of magnitude. In a later paper, Fedorov et al (1998), experiments were favorably compared directly with their theory. To demonstrate the agreement, Figure 12 (Figure 6 of Fedorov et al 1998) is presented.

V. FUTURE DIRECTION AND CONCLUDING REMARKS

The limiting form of standing gravity waves requires a more careful local analysis in space and time for various crest angles. In addition, it seems appropriate to seek a class of standing waves where the kinetic energy never becomes zero.

Major improvements to contact-line models are necessary for additional progress in low-mode Faraday waves. This could explain why damping rates measured experimentally are much larger than the predictions. In addition, strong nonlinearity in Faraday wave simulations has been unexplored, largely because of numerical limitations and an adequate model for wave breaking. This limitation precludes a careful study of the interesting subharmonic dynamics seen in the experiments. Wave breaking (spilling) in small waves is subtler and less well understood than plunging or spilling gravity waves. Breaking wave dissipation is

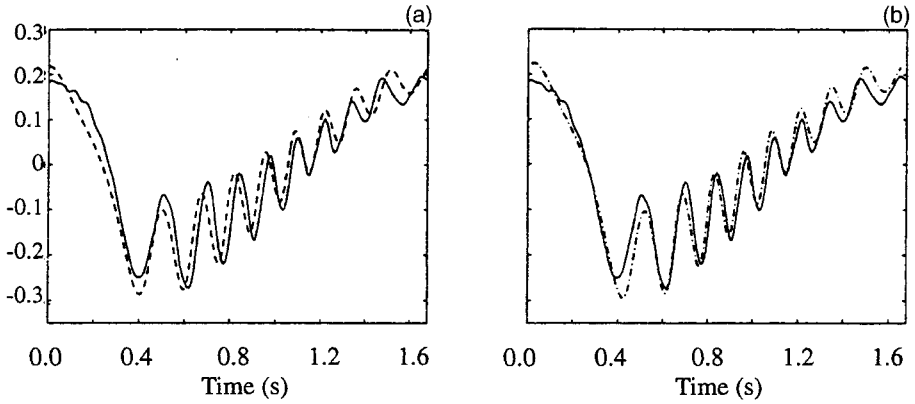

Figure 12 Experimental measurements of the slope of 6 Hz waves (solid line) compared to numerical solutions of Fedorov & Melville (1998). (a) Dash line is the Class 1 solution for an underlying wavelength of 5.2 cm, wave steepness of 0.20, and a nondimensional pressure-forcing amplitude of 0.0015. (b) Class 2 solution is the dot-dash line, wavelength of 5.1 cm, wave steepness of 0.205, and nondimensional pressure-forcing amplitude of 0.005. (Reproduced with permission.)

likely to be an important topic for nonlinear water wave studies in the foreseeable future.

The crest-roller issue remains largely unresolved for steep parasitic capillary wave generation in the absence of wind. The effects of vorticity on the parasitic capillaries, the underlying wave, and the attendant flow field require further study. Measurements such as Lin & Perlin (1999) of the flow beneath parasitic capillaries are required. Theoretical investigations that remove the spatial and temporal restrictions are also necessary.

ACKNOWLEDGMENTS

We thank the Office of Naval Research and the National Aeronautics & Space Administration for their long-term support as well as the University of Michigan. WWS gratefully acknowledges the Institute for Theoretical Geophysics of the Department of Applied Mathematics & Theoretical Physics of Cambridge University for sabbatical support during the writing of this review.

LITERATURE CITED

Banner ML, Peregrine DH. 1993. Wave breaking in deep water. *Annu. Rev. Fluid Mech.* 25:373–97

Bechhoefer J, Johnson B. 1996. A simple model for Faraday waves. *Am. J. Phys.* 64:1482–87

Bechhoefer J, Ego V, Manneville S, Johnson B. 1995. An experimental study of the onset of parametrically pumped surface waves in viscous fluids. *J. Fluid Mech.* 288:325–50

Benjamin TB, Scott JC. 1979. Gravity-capillary waves with edge constraints. *J. Fluid Mech.* 92:241–67

Benjamin TB, Ursell F. 1954. The stability of the plane free surface of a liquid in vertical periodic motion. *Proc. R. Soc. Lond. A* 225:505–15

Binks D, van de Water W. 1997. Nonlinear pattern formation of Faraday waves. *Phys. Rev. Lett.* 78:4043–46

Binks D, Westra M-T, van de Water W. 1997. Effect of depth on the pattern formation of Faraday waves. *Phys. Rev. Lett.* 79:5010–13

Bosch E, Lambermont H, van de Water W. 1994. Average patterns in Faraday waves. *Phys. Rev. E* 4:R3580–R83

Bosch E, van de Water W. 1993. Spatiotemporal intermittency in the Faraday experiment. *Phys. Rev. Lett.* 2:3420–23

Cerda EA, Tirapegui EL. 1998. Faraday's instability in viscous fluid. *J. Fluid Mech.* 368:195–228

Chen X-N, Wei R-J. 1994. Dynamic behavior of a non-propagating soliton under a periodically modulated oscillation. *J. Fluid Mech.* 259:291–303

Chossat P, Dias F. 1995. The 1:2 resonance with O(2) symmetry and its applications in hydrodynamics. *Nonlinear Sci.* 5:105–29

Christiansen B, Alstrøm P, Levinsen MT. 1995. Dissipation and ordering in capillary waves at high aspect ratios. *J. Fluid Mech.* 291:323–41

Cocciaro B, Faetti S, Nobili M. 1991. Capillarity effects on surface gravity waves in a cylindrical container: wetting boundary condition. *J. Fluid Mech.* 231:325–43

Concus P. 1962. Standing capillary-gravity waves of finite amplitudes. *J. Fluid Mech.* 14:568–76

Cox CS. 1958. Measurements of slopes of high-frequency wind waves. *J. Mar. Res.* 213:95–109

Craik ADD, Armitage JGM. 1995. Faraday excitation, hysteresis and wave instability in a narrow rectangular wave tank. *Fluid Dyn. Res.* 15:29–143

Crapper GD. 1957. An exact solution for progressive capillary waves of arbitrary amplitude. *J. Fluid Mech.* 2:532–40

Crapper GD. 1970. Non-linear capillary waves generated by steep gravity waves. *J. Fluid Mech.* 40:149–59

Crawford JD, Gollub JP, Lane D. 1993. Hidden symmetries of parametrically forced waves. *Nonlinearity* 6:119–64

Crawford JD. 1991. Normal forms for driven surface waves: Boundary conditions, symmetry, and genericity. *Physica D* 52:429–57

Crawford JD, Knobloch E, Riecke H. 1990. Period-doubling mode interactions with circular symmetry. *Physica D* 44:340–96

Debiane M, Kharif C. 1996. A new limiting form for steady periodic gravity waves with surface tension on deep water. *Phys. Fluids* 8:2780–2.

Decent SP. 1997. Solitary waves and chaotic twisting in a PDE model of Faraday resonance. *Fluid Dyn. Res.* 21:115–37

Decent SP, Craik ADD. 1995. Hysteresis in Faraday resonance. *J. Fluid Mech.* 293:237–68

Decent SP, Craik ADD. 1997. On limit cycles arising from the parametric excitation of standing waves. *Wave Motion* 25:275–94

Dias F, Bridges TJ. 1990. The third-harmonic resonance for capillary-gravity waves with O(2) spatial symmetry. *Stud. Appl. Math.* 82:13–35

Dias F, Kharif C. 1999. Nonlinear gravity and capillary-gravity waves. *Annu. Rev. Fluid Mech.* 31:301–46

Douady S. 1990. Experimental study of the Faraday instability. *J. Fluid Mech.* 221:383–409

Duncan JH, Philomin V, Behres M, Kimmel J. 1994. The formation of spilling breaking waves. *Phys. Fluids* 6:2558–60

Dussan V, EB. 1979. On the spreading of liquids on solid surfaces: static and dynamic

contact lines. *Annu. Rev. Fluid Mech.* 11:371–400

Ebuchi N, Kawamura H, Toba Y. 1987. Fine structure of laboratory wind-wave surfaces studied using an optical method. *Boundary-Layer Met.* 39:133–51

Edwards WS, Fauve S. 1993. Parametrically excited quasicrystalline surface waves. *Phys. Rev. E* 47:R788–91

Edwards WS, Fauve S. 1994. Patterns and quasi-patterns in the Faraday experiment. *J. Fluid Mech.* 278:123–48

Faraday M. 1831. On the forms and states assumed by fluids in contact with vibrating elastic surfaces. *Philos. Trans. R. Soc. Lond.* 52:319–40

Fauve S, Kumar K, Larouche C, Beysens D, Garrabos Y. 1992. Parametric instability of a liquid-vapour interface close to the critical point. *Phys. Rev. Lett.* 68:3160–63

Fedorov AV, Melville WK. 1998. Nonlinear gravity-capillary waves with forcing and dissipation. *J. Fluid Mech.* 354:1–42.

Fedorov AV, Melville WK, Rozenberg A. 1998. An experimental and numerical study of parasitic capillary waves. *Phys. Fluids* 10:1315–23

Feng ZC, Wiggins S. 1995. Fluid particle dynamics and Stokes drift in gravity and capillary waves generated by the Faraday instability. *Nonlin. Dyn.* 8:141–60

Friedel H, Laedke EW, Spatschek KH. 1995. Bifurcations and nonlinear dynamics of surface waves in Faraday resonance. *J. Fluid Mech.* 284:341–58

Generalis SC, Nagata M. 1995. Faraday resonance in a two-liquid layer system. *Fluid Dyn. Res.* 15:145–65

Goodridge CL, Shi WT, Lathrop DP. 1996. Threshold dynamics of singular gravity-capillary waves. *Phys. Rev. Lett.* 76:1824–27

Goodridge CL, Shi WT, Hentschel HGE, Lathrop DP. 1997. Viscous effects in droplet-ejecting capillary waves. *Phys. Rev. E* 45:472–75

Goodridge CL, Hentschel HGE, Lathrop DP. 1999. Breaking Faraday waves: critical slowing of droplet ejection rates. *Phys. Rev. Lett.* 82:3062–65

Guthart GS, Wu TY-T. 1991. Observation of a standing kink cross wave parametrically excited. *Proc. R. Soc. Lond. A* 434:435–40

Hammack JL, Henderson DM. 1993. Resonant interactions among surface water waves. *Annu. Rev. Fluid Mech.* 25:55–97

Henderson D, Hammack J, Kumar P, Shah D. 1992. The effects of static contact angles on standing waves. *Phys. Fluids A* 4:2320–22

Henderson DM, Miles JW. 1991. Faraday waves in 2:1 internal resonance. *J. Fluid Mech.* 222:449–70

Henderson DM, Miles JW. 1994. Surface-wave damping in a circular cylinder with a fixed contact line. *J. Fluid Mech.* 275:285–99

Henderson DM, Miles JW. 1990. Single mode Faraday waves in small cylinders. *J. Fluid Mech.* 213:95–109

Hocking LM. 1987a. The damping of capillary-gravity waves at a rigid boundary. *J. Fluid Mech.* 179:253–66

Hocking LM. 1987b. Waves produced by a vertically oscillating plate. *J. Fluid Mech.* 179:267–81

Huh J. 1991. *A numerical study of capillary-gravity waves.* PhD dissertation, Applied Mechanics, Univ. Mich, Ann Arbor

Jiang L, Ting C-L, Perlin M, Schultz WW. 1996. Moderate and steep Faraday waves: instabilities, modulation and temporal asymmetries. *J. Fluid Mech.* 329:275–307

Jiang L, Perlin M, Schultz, WW. 1998. Period tripling and energy dissipation of breaking standing waves. *J. Fluid Mech.* 369:273–99

Jiang L, Lin H-J, Schultz WW, Perlin M. 1999. Unsteady ripple generation on steep gravity-capillary waves. *J. Fluid Mech.* 386:281–304

Kumar K. 1996. Linear theory of Faraday instability in viscous liquids. *Proc. R. Soc. Lond. A* 452:1113–26

Kumar K, Tuckerman LS. 1994. Parametric instability of the interface between two fluids. *J. Fluid Mech.* 279:49–68

Laedke EW, Spatschek KH. 1991. On localized solutions in nonlinear Faraday resonance. *J. Fluid Mech.* 223:589–601

Landsberg AS, Knobloch E. 1993. New types of waves in systems with O(2) symmetry. *Phys. Lett. A* 179:316–24

Landsberg AS, Knobloch E. 1996. Oscillatory bifurcation with broken translation symmetry. *Phys. Rev. E* 53:3579–3600

Larraza A, Putterman S. 1984. Theory of nonpropagating surface-wave solitons. *J. Fluid Mech.* 148:443–49

Lin HJ, Perlin M. 1998. Improved methods for thin, surface boundary layer investigations. *Exp. Fluids* 25:431–44

Lin HJ, Perlin M. 1999. The velocity and vorticity fields beneath gravity-capillary waves exhibiting parasitic ripples. *Phys. Fluids*. Under revision

Lioubashevski O, Fineberg J, Tuckerman LS. 1997. Scaling of the transition to parametrically driven surface waves in highly dissipative systems. *Phys. Rev. E* 55:R3832–3835

Longuet-Higgins MS. 1963. The generation of capillary waves by steep gravity waves. *J. Fluid Mech.* 16:138–59

Longuet-Higgins MS. 1992. Capillary rollers and bores. *J. Fluid Mech.* 240:659–79

Longuet-Higgins MS. 1994. Shear instability in spilling breakers. *Proc. R. Soc. Lond. A* 446:399–409

Longuet-Higgins MS. 1995. Parasitic capillary waves: a direct calculation. *J. Fluid Mech.* 301:79–107

Longuet-Higgins MS. 1996. Capillary jumps on deep water. *J. Phys. Ocean.* 26: 1957–65

Longuet-Higgins MS, Cleaver RP. 1994. Crest instabilities of gravity waves. Part 1. The almost-highest wave. *J. Fluid Mech.* 258:115–29

Longuet-Higgins MS, Dommermuth DG. 1997. Crest instabilities of gravity waves. Part 3. Nonlinear development and breaking. *J. Fluid Mech.* 336:33–50

Longuet-Higgins MS, Tanaka M. 1997. On the crest instabilities of steep surface waves. *J. Fluid Mech.* 336:51–68

Martel C, Knobloch E. 1997. Damping of nearly inviscid water waves. *Phys. Rev. E* 56:5544–48

Martel C, Nicolas JA, Vega JM. 1998. Surface-wave damping in a brimful circular cylinder. *J. Fluid Mech.* 360:213–28

Mercer GN, Roberts AJ. 1992. Standing waves in deep water: Their stability and extreme form. *Phys. Fluids A* 4:259–69

Mesquita ON, Kane S, Gollub JP. 1992. Transport by capillary waves: Fluctuating Stokes drift. *Phys. Rev. A* 45:3700–05

Miles JW. 1967. Surface wave damping in closed basins. *Proc. R. Soc. Lond. A* 297:459–75

Miles JW. 1984a. Nonlinear Faraday resonance. *J. Fluid Mech.* 146:285–302

Miles JW. 1984b. Parametrically excited solitary waves. *J. Fluid Mech.* 148:451–60

Miles J. 1990. Parametrically excited standing edge waves. *J. Fluid Mech.* 214:43–57

Miles J. 1991. The capillary boundary layer for standing waves. *J. Fluid Mech.* 222:197–205

Miles J. 1992. On surface waves with zero contact angle. *J. Fluid Mech.* 245:485–92

Miles JW. 1993. On Faraday waves. *J. Fluid Mech.* 248:671–83

Miles JW. 1994. Faraday waves: Rolls versus squares. *J. Fluid Mech.* 269:353–71

Miles JW, Henderson DM. 1990. Parametrically forced surface waves. *Annu. Rev. Fluid Mech.* 22:143–65

Miles JW, Zou Q-P. 1993. Parametric excitation of a detuned spherical pendulum. *J. Sound Vib.* 164:237–50

Milner ST. 1991. Square patterns and secondary instabilities in driven capillary waves. *J. Fluid Mech.* 225:81–100

Mui RCY, Dommermuth DG. 1995. The vortical structure of parasitic capillary waves. *J. Fluids Eng.* 117:355–61

Nagata M. 1989. Nonlinear Faraday resonance in a box with a square base. *J. Fluid Mech.* 209:265–84

Penney WG, Price AT. 1952. Finite periodic stationary gravity waves in a perfect fluid. *Proc. R. Soc. Lond A* 244:254–84

Perlin M, Hammack J. 1991. Experiments on ripple instabilities. Part 3: Resonant quartets of the Benjamin-Feir type. *J. Fluid Mech.* 229:229–68

Perlin M, Ting C-L. 1992. Steep gravity-capillary waves within the internal resonance regime. *Phys. Fluids A* 4:2466–78

Perlin M, Lin H-J, Ting C-L. 1993. On parasitic capillary waves generated by steep gravity waves: an experimental investigation with spatial and temporal measurements. *J. Fluid Mech.* 255:597–620

Perlin M, Bernal LP, He J. 1996. An experimental study of deep water plunging breakers. *Phys. Fluids* 8:2365–74

Rayleigh JWS. 1915. Deep water waves, progressive or stationary, to the third order of approximation. *Proc. R. Soc. Lond. A* 91:345–53

Ruvinsky KD, Feldstein FI, Freidman GI. 1991. Numerical simulations of the quasi-stationary stage of ripple excitation by steep gravity-capillary waves. *J. Fluid Mech.* 230:339–53

Schultz WW, Huh J, Griffin OM. 1994. Potential energy in steep and breaking waves. *J. Fluid Mech.* 278:201–28

Schultz WW, Vanden-Broek J-M, Jiang L, Perlin M. 1998. Highly nonlinear standing waves with small capillary effect. *J. Fluid Mech.* 369:253–72

Schwartz LW, Fenton JD. 1982. Strongly nonlinear waves. *Annu. Rev. Fluid Mech.* 14:39–60

Schwartz LW, Vanden-Broeck J-M. 1979. Numerical solutions of the exact equations for capillary-gravity waves. *J. Fluid Mech.* 95:119–39

Schwartz LW, Whitney AK. 1981. A semi-analytical solution for nonlinear standing waves in deep water. *J. Fluid Mech.* 107:147–71

Simonelli F, Gollub JP. 1989. Surface wave mode interactions: effects of symmetry and degeneracy. *J. Fluid Mech.* 199:471–94

Smith MK, James A, Vukasinovic B, Glezer A. 1998. Vibration-induced droplet atomization. *Proc. Fourth Int. Microgravity Fluid Phys. Trans. Phenomena Conf.,* NASA Lewis Res. Cent., Cleveland, OH

Sobey RJ. 1986. Wind-wave prediction. *Annu. Rev. Fluid Mech.* 18:149–72

Stokes GG. 1880. Considerations relative to the greatest height of oscillatory irrotational waves which can be propagated without change of form. *Math. Phys. Papers* 1:225–28

Taylor GI. 1953. An experimental study of standing waves. *Proc. R. Soc. Lond. A* 218:44–59

Tsai C-P, Jeng D-S. 1994. Numerical Fourier solutions of standing waves in finite water depth. *Appl. Ocean Res.* 16:185–93

Tulin MP, Li JJ. 1991. A mechanism for wave deformation and breaking intermediated by resonant sidebands. *Proc. IUTAM Sympos. Breaking Waves,* Ed. ML Banner, RHJ Grimshaw Springer:21–37

Umeki M. 1991. Faraday resonance in rectangular geometry. *J. Fluid Mech.* 227:161–92

Umeki M, Kambe T. 1989. Nonlinear dynamics and chaos in parametrically excited surface waves. *J. Phys. Soc. Jpn.* 48:140–54

Vanden-Broeck J-M. 1984. Nonlinear gravity-capillary standing waves in water of arbitrary uniform depth. *J. Fluid Mech.* 139:97–104

Wang X, Wei R. 1994. Observations of collision behavior of parametrically excited standing solitons. *Phys. Lett. A* 192:1–4

Watson KM, McBride JB. 1993. Excitation of capillary waves by longer waves. *J. Fluid Mech.* 250:103–19

Watson KM, Buchsbaum SB. 1996. Interaction of capillary waves with longer waves. Part 1. General theory and specific applications to waves in one dimension. *J. Fluid Mech.* 321:87–120

Wilton JR. 1915. On ripples, *Phil. Mag.* (6) 29:688–700

Wu J, Keolian R, Rudnick I. 1984. Observation of a non-propagating hydrodynamic soliton. *Phys. Rev. Lett.* 52:1421–24

Yoshimatsu K, Funakoshi M. 1998. Primary patterns in Faraday surface waves at high aspect ratio. *J. Phys. Soc. Jpn.* 67:451–61

Zhang W, Viñals J. 1997. Pattern formation in weakly damped parametric surface waves. *J. Fluid Mech.* 336:301–30

Zhang X. 1995. Capillary-gravity and capillary waves generated in a wind wave tank: observations and theories. *J. Fluid Mech.* 289:51–82

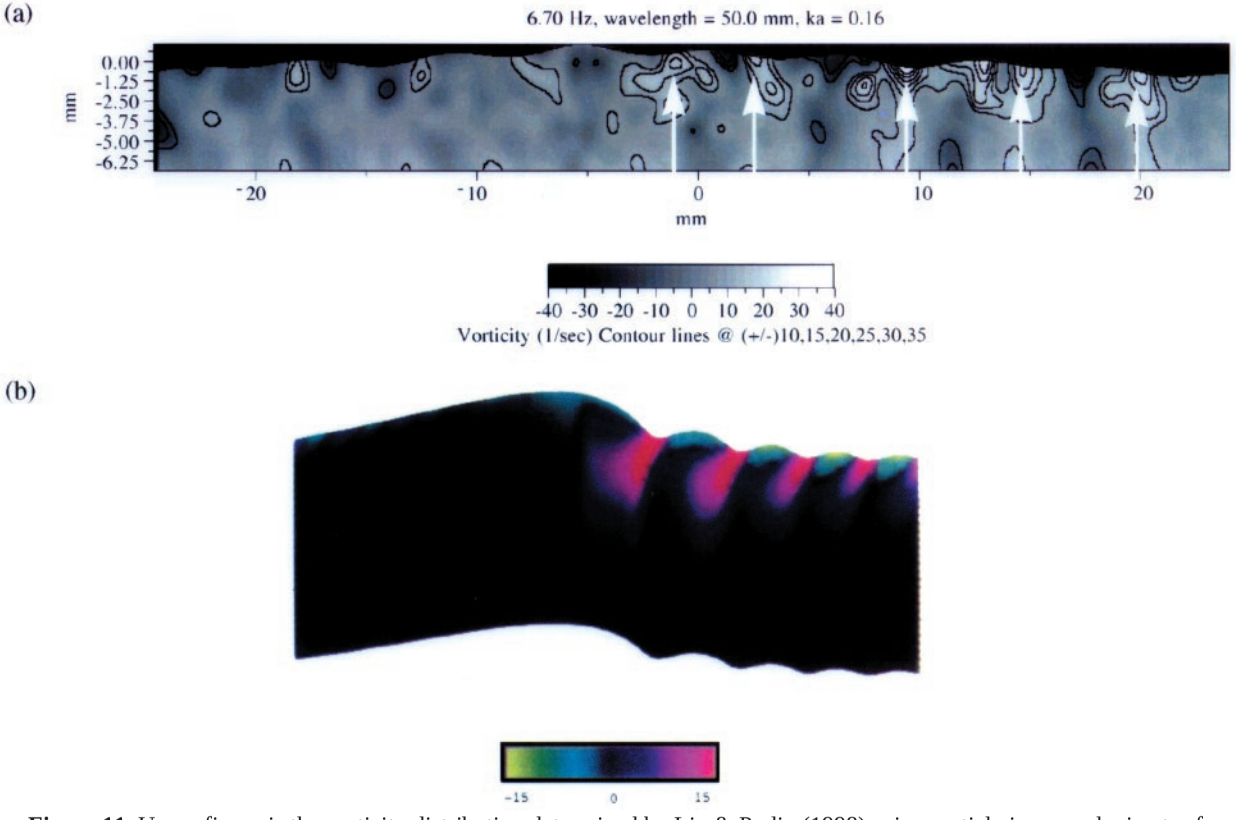

Figure 11 Upper figure is the vorticity distribution determined by Lin & Perlin (1998) using particle image velocimetry for a 5-cm long primary wave with a steepness 0.16. Lower figure is the subsurface vorticity structure (their figure 8) calculated by Mui & Dommermuth (1995). (Reproduced with permission).

Annual Review of Fluid Mechanics
Volume 32, 2000

CONTENTS